symmetry

MDPI

Article

Analytical Analyses for a Fractional Low-Pass Electrical Transmission Line Model with Dynamic Transition

Hassan Almusawa [1,*], Adil Jhangeer [2] and Maham Munawar [3]

[1] Department of Mathematics, College of Sciences, Jazan University, Jazan 45142, Saudi Arabia
[2] Department of Mathematics, Namal University, Mianwali 42250, Pakistan; adil.jhangeer@namal.edu.pk
[3] Department of Mathematics, University of Central Punjab, Lahore 54000, Pakistan; maham.munawar@ucp.edu.pk
* Correspondence: haalmusawa@jazanu.edu.sa

Abstract: This research explores the solitary wave solutions, including dynamic transitions for a fractional low-pass electrical transmission (LPET) line model. The fractional-order (FO) LPET line mathematical system has yet to be published, and neither has it been addressed via the extended direct algebraic technique. A computer program is utilized to validate all of the incoming solutions. To illustrate the dynamical pattern of a few obtained solutions indicating trigonometric, merged hyperbolic, but also rational soliton solutions, dark soliton solutions, the representatives of the semi-bright soliton solutions, dark singular, singular solitons of Type 1 and 2, and their 2D and 3D trajectories are presented by choosing appropriate values of the solutions' unrestricted parameters. The effects of fractionality and unrestricted parameters on the dynamical performance of achieved soliton solutions are depicted visually and thoroughly explored. We furthermore discuss the sensitivity assessment. We, however, still examine how our model's perturbed dynamical framework exhibits quasi periodic-chaotic characteristics. Our investigated solutions are compared with those listed in published literature. This research demonstrates the approach's profitability and effectiveness in extracting a range of wave solutions to nonlinear evolution problems in mathematics, technology, and science.

Keywords: conformal fractional derivative; new extended algebraic method; soliton solutions; nonlinear low-pass electrical transmission line

Citation: Almusawa, H.; Jhangeer, A.; Munawar, M. Analytical Analyses for a Fractional loW-Pass Electrical Transmission Line Model with Dynamic Transition. *Symmetry* **2022**, *14*, 1377. https://doi.org/10.3390/sym14071377

Academic Editor: Yakup Yildirim

Received: 10 May 2022
Accepted: 21 June 2022
Published: 4 July 2022

1. Introduction

The extraction of solutions based on propagating waves to integer-order nonlinear evolution equations (NLEEs) has progressed, surpassing estimates. NLEEs of FO have attracted attention in recent decades as a result of their suitability in genuine applications as classical numerical methods based on integer-order derivatives, especially nonlinear systems, fail to improve well in many situations [1]. Fractional calculus, which was introduced in 1965, is employed to represent the issue regulating FO-NLEEs [2] and is thought to be involved in the numerous innovations happening in various sectors of technology and modern science [3]. As a consequence, especially the development of symbolic computing programs such as Maple throughout the past few decades, it has attracted a deal of interest among modern sciences [4]. Several representations for introducing a calculus have been described, including conformable derivation, fractional Riemann–Liouville derivative, beta derivative, Atangana's conformable derivative, Caputo–Fabrizio derivative, Riesz and Weyl derivatives, and so on [5,6]. Non-locality, as well as heredity, are two standard features of fractional derivatives (FDs) formulas [7], which depart significantly from the Newton–Leibniz calculus [8]. FD concepts and some essential formulations can convert fractional nonlinear partial differential equations (PDEs) into nonlinear integer-order ordinary differential equations (ODEs).

In terms of FD concepts, conformable derivation (CD) established by Khalil et al. [9] piqued the researcher's curiosity [10] due to numerous advantages over other FDs [11]. To predict the actual solution to NLEEs of FO, a broad range of trustworthy techniques has been recommended. Among the successful approaches are the homotopy analysis method [12], the fractional reduced differential transform methods [13], the homotopy perturbation technique [14], and the fractional iterative method [15]. The adomian decomposition method [16], the $\left(\frac{G'}{G^2}\right)$-expansion technique [17], exp function technique [18], modified simple equation technique [19,20], the solitary ansatz technique [20], and the extended tanh–coth technique [20], the modified Kudryshov approach [21], extended sinh–Gordon expansion approach [22], auxiliary equation approach [23], new auxiliary equation approach [24] and so forth. It is essential to note that a new auxiliary equation approach is used in ref. [24]. Notwithstanding all of the initiatives for the solution of nonlinear FDEs using diverse approaches, a consistent approach remains elusive. With many of the approaches, the newly suggested innovative analytical $\left(\frac{G'}{G^2}\right)$-expansion method [25] has received significant attention due to its flexibility and applicability.

Investigating a family of temporal time-FNEE models, including time-FCDs, is essential in many nonlinear wave dispersion situations. In addition, to do this, a highly accurate semi-analytical technique is created as well as constructed with the residual error factors in mind towards addressing a category of fifth-order time-FCKdVEs [26]. This work [27] investigates the dynamical activity with its dispersive extended nonlinear Schrödinger equation (NLSE). A novel ϕ_6 model expansion approach is employed to investigate unique solitary waveforms of such investigated model. The essential purpose of this strategy is to establish a medium enabling Jacobian elliptic formulations by incorporating numerous parameters. Investigators create a stochastic approach to address a FO differential system focused on breast cancer progression during the immune-chemotherapeutic therapy phase [28]. The former work [29] investigates two distinct models: the NLSE exhibiting power-law non-linearities as well as the (3 + 1)-D NLSE. We are engaged in the nonlinear Kadomtsev–Petviashvili equation (KP) with competitive dispersion. Furthermore, the overall stability of the related dynamical network is explored by employing phase plane theory [30]. Specialists established throughout this research study that wave profiles vary with changes in the fundamental attributes affiliated to phenomena and are influenced mainly by linear impacts [31]. The topic of optical solitons is intriguing because soliton solutions have been examined in numerous mathematical physics models. Observing optical solitons is one of the most important aspects of nonlinear fibre optics. In applied science and engineering, soliton has a number of uses. Nonlinear differential equations can be solved using a variety of strategies. The new extended direct algebraic technique provides such illustration[32–34].

The entirety of such a composition is structured as follows: The model description and system of algebraic equations, along with the corresponding solution set, may be found in the Section 2 "Mathematical Configuration". Section 3 "Implementation of the Extended Direct Algebraic Method" discusses the expansion method's application to the FO-LPET line model. In Section 3 "Sufficient Conditions for the Stability of the Results", the stability and sufficient conditions of outcomes are discussed. Section 4 "Graphical Interface Structure for the Results" offers a discussion of some of the investigated results with the sensitivity assessment and quasiperiodic behaviors in subsections. In Section 5, there is a discussion and results analysis about the influence of free parameters as well as fractionality factor. In Section 6, we discussed a comparative analysis via different FDs. Ultimately, in the Section 7, a broad conclusion of the study is provided.

2. Mathematical Configuration

The space-time FDE regulating wave propagation in LPET lines will be solved using the extended direct algebraic technique. We consider the FO-LPET line model as follows in order to use the extended direct algebraic approach to create the exact results of the space-time fractional LPET line model:

$$C_0LD_{tt}^{2\alpha}v(x,t) - D_{xx}^{2\alpha}v(x,t) - \frac{\delta^2}{12}D_{xxxx}^{4\alpha}v(x,t) - C_0L\nu D_{tt}^{2\alpha}v^2(x,t) + C_0L\beta D_{tt}^{2\alpha}v^3(x,t) = 0, \quad (1)$$

in which δ, ν and β are the aforementioned constants, and $D_t^\alpha v$ and $D_x^\alpha v$ indicates the conformal derivative (CD) [9] of $v(x,t)$ of FO α as for regard to t and x, correspondingly. The variable x represents the propagation distance, while the value t provides the slow time. It is worth noting that Equation (1) is identical towards the space–time FDE guiding direction of dispersion in the low–pass electrical transmission $(LPET)$ line described in refs. [3,35] if $LC_0 = 1$ is taken into account.

Employing this same transformation $v(x,t) = V(\xi)$, $\xi = \mu\frac{x^\alpha}{\alpha} + \sigma\frac{t^\alpha}{\alpha}$, (where σ and μ are non zero parameters) for Equation (1). By trying to integrate the resultant equation two times with regard to and reducing the constants to zero, one can get the ensuing ODE:

$$(C_0L\sigma^2 - \mu^2)V - C_0L\nu\sigma^2V^2 + C_0L\beta\sigma^2V^3 - \frac{\delta^2\mu^4}{12}V'' = 0, \quad (2)$$

where $V' = \frac{dV}{d\xi}$, i-e prime indicates derivative with respect to independent variable ξ.

3. Implementation of the Extended Direct Algebraic Method

The whole portion provides a concise but thorough overview as well as implementation of the present approach [32–34]. We analyze the nonlinear fractional PDEs listed below:

$$u^*(v, D_t^\alpha v, D_x^\alpha v, D_t^{2\alpha}v, D_t^\alpha D_x^\alpha v, D_x^{2\alpha}v) = 0, \alpha > 0, t \geq 0, \quad (3)$$

$v(x,t)$ is the unspecified independent variables' function x and t in Equation (3), where u^* is a polynomial of v as well as its partial FDs. The preceding procedures must be taken to investigate an exact solution based on the traveling waves of Equation (3). In most cases, a linear fractional transformation is employed. That would be $v(x,t) = V(\xi)$, $\xi = \mu\frac{x^\alpha}{\alpha} + \sigma\frac{t^\alpha}{\alpha}$, Where σ and μ are non zero parameters. It might be beneficial to convert Equation (3) to another ODE, as shown underneath.

$$U(V, V', V'', ...) = 0. \quad (4)$$

Thus, prime denotes the derivative of ξ. According to this technique, the general solution approaches Equation (4) as the solution:

$$V(\xi) = b_0 + \sum_{i=1}^{N}\left[b_iP(\xi)^i\right], \quad (5)$$

where

$$P'(\xi) = ln(\rho)\Big(m_1 + m_2P(\xi) + m_3P^2(\xi)\Big), \quad \rho \neq 0, 1 \quad (6)$$

as of m_1, m_2, and m_3 represent real fixed quantities thus N could be derived by balancing the nonlinear components as well as the largest order derivative in Equation (4).

We acquire balancing coefficient $N = 1$ by comparing the highest power of nonlinear term V^3 with the highest order derivative term V'' from Equation (2) that relates towards the assumed solution pattern (Equation (5)):

$$V_j(\xi) = b_0 + b_1P_j(\xi), \qquad \text{for } j = 0,\ 1,\ 2, ... \quad (7)$$

where $P(\xi)$ satisfies Equation (6). When plugging Equation (7) into Equation (2) then comparing the coefficients of distinct powers of $P^r(\xi)$, $(r = 0,\ 1,\ 2,\ 3)$ to zero, we would achieve the following algebraic equation system:

$$\begin{aligned}
P^0(\xi):\ & 12\delta^2\mu^4 b_1^2 m_1^2 \ln\rho^2 - 72LC_0\beta\sigma^2 b_0^4 + 96LC_0\nu\sigma^2 b_0^3 \\
& - 12\delta^2\mu^4 b_0^2 LC_0\sigma^2 + 12\delta^2\mu^6 b_0^2 + c = 0, \\
P^1(\xi):\ & 24\delta^2\mu^4 b_1^2 m_1 \ln\rho^2 m_2 - 288LC_0\beta\sigma^2 b_0^3 b_1 + 288LC_0\nu\sigma^2 b_0^2 b_1 \\
& - 24\delta^2\mu^4 b_0 b_1 LC_0\sigma^2 + 24\delta^2\mu^6 b_0 b_1 = 0, \\
P^2(\xi):\ & 24\delta^2\mu^4 b_1^2 m_1 \ln\rho^2 m_3 + 12\delta^2\mu^4 b_1^2 m_2^2 \ln\rho^2 - 432LC_0\beta\sigma^2 b_0^2 b_1^2 \\
& + 288LC_0\nu\sigma^2 b_0 b_1^2 - 12\delta^2\mu^4 b_1^2 LC_0\sigma^2 + 12\delta^2\mu^6 b_1^2 = 0, \\
P^3(\xi):\ & 24\delta^2\mu^4 b_1^2 m_1 \ln\rho^2 m_3 - 288LC_0\beta\sigma^2 b_0 b_1^3 + 96LC_0\nu\sigma^2 b_1^3 = 0, \\
P^4(\xi):\ & 12\delta^2\mu^4 b_1^2 m_3^2 \ln\rho^2 - 72LC_0\beta\sigma^2 b_1^4 = 0.
\end{aligned}$$

After, we evaluate the preceding equations for the parameters σ, and μ, we would achieve corresponding solution set:

$$\begin{aligned}
\sigma &= \pm\frac{18\nu}{(9\beta - 2\nu^2)\delta\ln\rho}\left[\sqrt{\frac{2\beta}{3LC_0m_2^2 - 12LC_0m_1m_3}}\right], \\
\mu &= \pm\frac{2\nu}{\delta\ln\rho}\left[\sqrt{\frac{6}{8\nu^2m_1m_3 - 2\nu^2m_2^2 - 36\beta m_1m_3 + 9\beta m_2^2}}\right], \\
b_0 &= \frac{\nu}{3\beta}\theta, \qquad b_1 = \frac{2m_3\nu}{3m_2\beta}\theta, \qquad \text{where:}\quad \theta = \left[\frac{4m_1m_3 - m_2^2 \pm \sqrt{-4m_1m_2^2m_3 + m_2^4}}{(4m_1m_3 - m_2^2)}\right].
\end{aligned}$$

The following are general solutions to Equation (6) for the parameters m_1, m_2, and m_3, whereby $\Theta_1 = (m_2^2 - 4m_1m_3)$.

Case 1. If $\Theta_1 < 0$ and $m_3 \neq 0$, then

After that, by inserting the values of b_0, and b_1 into Equation (7), it will offer the corresponding results for this same integrated equation, i.e., Equation (2) and thereafter, using the transformation $V(\xi) = v(x,t)$, since $\xi = \mu\frac{x^\alpha}{\alpha} + \sigma\frac{t^\alpha}{\alpha}$, this would eventually provide the solution to Equation (1):

$$V_1^* = \frac{\nu}{3\beta}\theta + \frac{2m_3\nu}{3m_2\beta}(\theta - 1)\left(-\frac{m_2}{2m_3} + \frac{\sqrt{-\Theta_1}}{2m_3}\tan_\rho\left(\frac{\sqrt{-\Theta_1}}{2}\left[\mu\frac{x^\alpha}{\alpha} + \sigma\frac{t^\alpha}{\alpha}\right]\right)\right),$$

or

$$V_1 = \frac{\nu}{3\beta}\theta + \frac{2m_3\nu}{3m_2\beta}(\theta - 1)\left(-\frac{m_2}{2m_3} + \frac{\sqrt{-\Theta_1}}{2m_3}\tan_\rho\left(\frac{\sqrt{-\Theta_1}}{2}\xi\right)\right).$$

As a result, the corresponding solutions are retrieved, operating along virtually similar patterns.

$$V_2 = \frac{\nu}{3\beta}\theta + \frac{2m_3\nu}{3m_2\beta}(\theta - 1)\left(-\frac{m_2}{2m_3} - \frac{\sqrt{-\Theta_1}}{2m_3}\cot_\rho\left(\frac{\sqrt{-\Theta_1}}{2}\xi\right)\right),$$

$$V_3 = \tfrac{\nu}{3\beta}\theta + \tfrac{2m_3\nu}{3m_2\beta}(\theta - 1)\left(-\tfrac{m_2}{2m_3} + \tfrac{\sqrt{-\Theta_1}}{2m_3}\left(\tan_\rho\left(\sqrt{-(\Theta_1)}\xi\right) \pm \sqrt{mn}\sec_\rho\left(\sqrt{-(\Theta_1)}\xi\right)\right)\right),$$

$$V_4 = \frac{\nu}{3\beta}\theta + \frac{2m_3\nu}{3m_2\beta}(\theta-1)\left(-\frac{m_2}{2m_3} + \frac{\sqrt{-\Theta_1}}{2m_3}\left(\cot_\rho\left(\sqrt{-\Theta_1}\xi\right) \pm \sqrt{mn}\,\csc_\rho\left(\sqrt{-\Theta_1}\xi\right)\right)\right),$$

$$V_5 = \frac{\nu}{3\beta}\theta + \frac{2m_3\nu}{3m_2\beta}(\theta-1)\left(-\frac{m_2}{2m_3} + \frac{\sqrt{-\Theta_1}}{4m_3}\left(\tan_\rho\left(\frac{\sqrt{-\Theta_1}}{4}\xi\right) - \cot_\rho\left(\frac{\sqrt{-\Theta_1}}{4}\xi\right)\right)\right).$$

Case 2. If $\Theta_1 > 0$ and $m_3 \neq 0$, then

$$V_6 = \frac{\nu}{3\beta}\theta + \frac{2m_3\nu}{3m_2\beta}(\theta-1)\left(-\frac{m_2}{2m_3} - \frac{\sqrt{\Theta_1}}{2m_3}\tanh_\rho\left(\frac{\sqrt{\Theta_1}}{2}\xi\right)\right),$$

$$V_7 = \frac{\nu}{3\beta}\theta + \frac{2m_3\nu}{3m_2\beta}(\theta-1)\left(-\frac{m_2}{2m_3} - \frac{\sqrt{\Theta_1}}{2m_3}\coth_\rho\left(\frac{\sqrt{\Theta_1}}{2}\xi\right)\right),$$

$$V_8 = \tfrac{\nu}{3\beta}\theta + \tfrac{2m_3\nu}{3m_2\beta}(\theta-1)\left(-\tfrac{m_2}{2m_3} + \tfrac{\sqrt{\Theta_1}}{2m_3}\left(-\tanh_\rho\left(\sqrt{\Theta_1}\xi\right) \pm \sqrt{-mn}\,\mathrm{sech}_\rho\left(\sqrt{\Theta_1}\xi\right)\right)\right),$$

$$V_9 = \frac{\nu}{3\beta}\theta + \frac{2m_3\nu}{3m_2\beta}(\theta-1)\left(-\frac{m_2}{2m_3} + \frac{\sqrt{\Theta_1}}{2m_3}\left(-\coth_\rho\left(\sqrt{\Theta_1}\xi\right) \pm \sqrt{mn}\,\mathrm{csch}_\rho\left(\sqrt{\Theta_1}\xi\right)\right)\right),$$

$$V_{10} = \frac{\nu}{3\beta}\theta + \frac{2m_3\nu}{3m_2\beta}(\theta-1)\left(-\frac{m_2}{2m_3} - \frac{\sqrt{\Theta_1}}{4m_3}\left(\tanh_\rho\left(\frac{\sqrt{\Theta_1}}{4}\xi\right) + \coth_\rho\left(\frac{\sqrt{\Theta_1}}{4}\xi\right)\right)\right).$$

Case 3. If $m_1 = 0$ and $m_2 \neq 0$ then

$$V_{11} = \frac{2m_3\nu}{3m_2\beta}\left(\frac{mm_2}{m_3\left(\cosh_\rho(m_2\xi) - \sinh_\rho(m_2\xi) + m\right)}\right),$$

$$V_{12} = \frac{2m_3\nu}{3m_2\beta}\left(\frac{m_2\left(\sinh_\rho(m_2\xi) + \cosh_\rho(m_2\xi)\right)}{m_3\left(\sinh_\rho(m_2\xi) + \cosh_\rho(m_2\xi) + n\right)}\right).$$

Case 4. If $m_2 = p, m_3 = pq,\ (q \neq 0$ and $m_1 = 0)$ then

$$V_{13} = \frac{2m_3\nu}{3m_2\beta}\left(\frac{m\rho^{p\xi}}{m - qn\rho^{p\xi}}\right).$$

Sufficient Conditions for the Stability of the Results

In mathematics, stability refers to the situation where a minor disruption inside a system does not have a significant impact on the system. In physical problems, solution stability is essential because if minor deviations from the mathematical model induced by unavoidable measurement errors have no correspondingly minor influence upon that solution, the mathematical equations characterizing the dilemma will fail to foretell the prospective outcome precisely.

As we have solitary wave solutions, the sufficient conditions for stability are as follows:

- $\frac{2\beta}{3LC_0m_2^2 - 12LC_0m_1m_3} > 0$, for σ
- $\frac{6}{8\nu^2m_1m_3 - 2\nu^2m_2^2 - 36\beta m_1m_3 + 9\beta m_2^2} > 0$, for μ
- $m_2^4 - 4m_1m_2^2m_3 > 0$, for θ .

4. Graphical Interface Structure for the Results

This entire section is centered on highlighting the representational assessment of some of the key findings from this study. It is worth mentioning that wave propagation spans several types of soliton solutions. Because V_6 represents dark class soliton solutions. V_8 is associated with the semi-bright soliton solution group, and the soliton solutions

associated with the dark-singular type are V_{10}, but V_9 is associated with the class of singular results of *Type* 1 and 2, while V_7 is associated with the type of singular solution of *Type* 2. Figures 1–8 depict 2D visuals, 3D graphics, and 2D contour graphics of a handful of the soliton solutions for different parameters.

Figures 1 and 2:

One such diagram depicts a physical understanding of V_6 as it pertains to the domain of dark solutions. Here is a graphical representation of the examination using the parameters, $b_0 = 0.10714$, $b_1 = -0.03174$, $\mu = \sigma = 1, \nu = -0.0025$, $\beta = 0.035$, $\rho = e$, $m_1 = 1$, $m_2 = 3$, $m_3 = 2$ with in the interval $(0, 2)$.

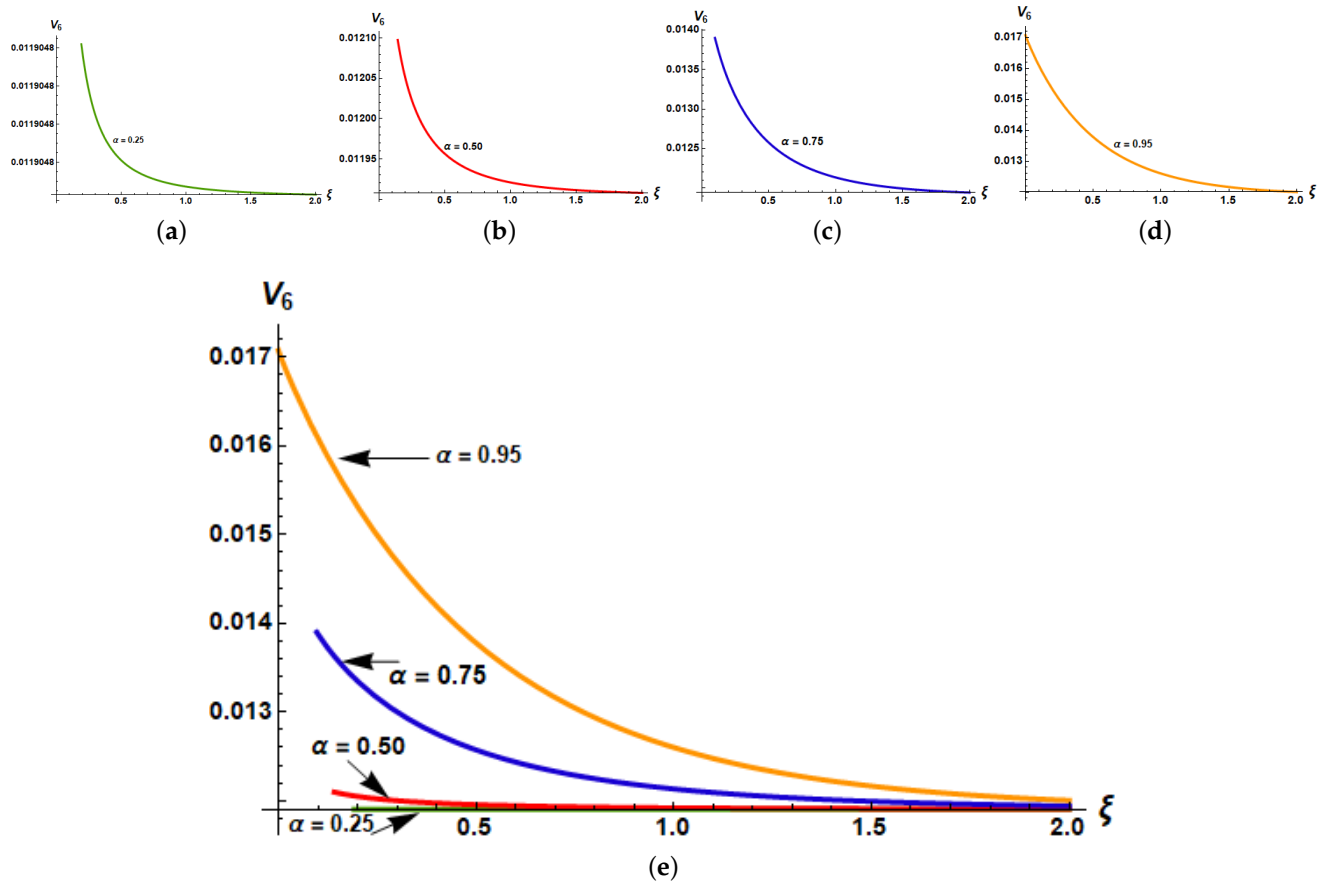

Figure 1. 2D-Graphical representation for V_6. (**a**) $\alpha = 0.25$. (**b**) $\alpha = 0.50$. (**c**) $\alpha = 0.75$. (**d**) $\alpha = 0.95$. (**e**) Combine effect for different fractional values of α.

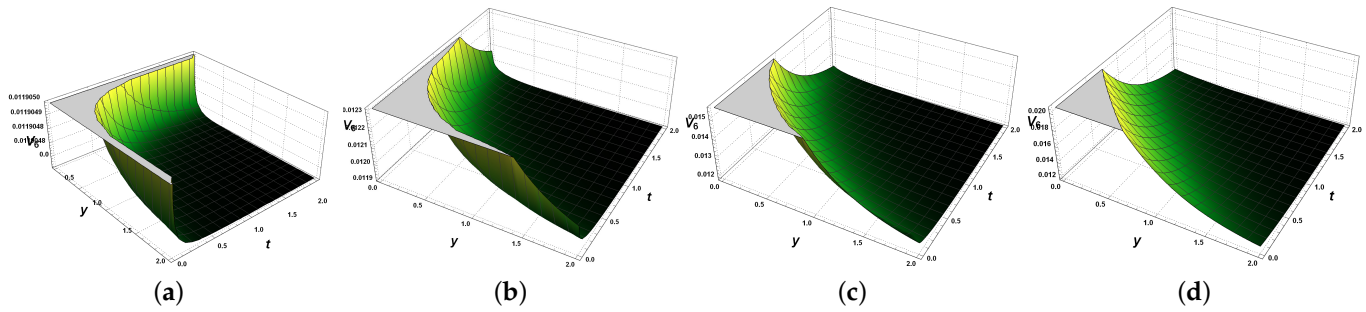

Figure 2. *Cont.*

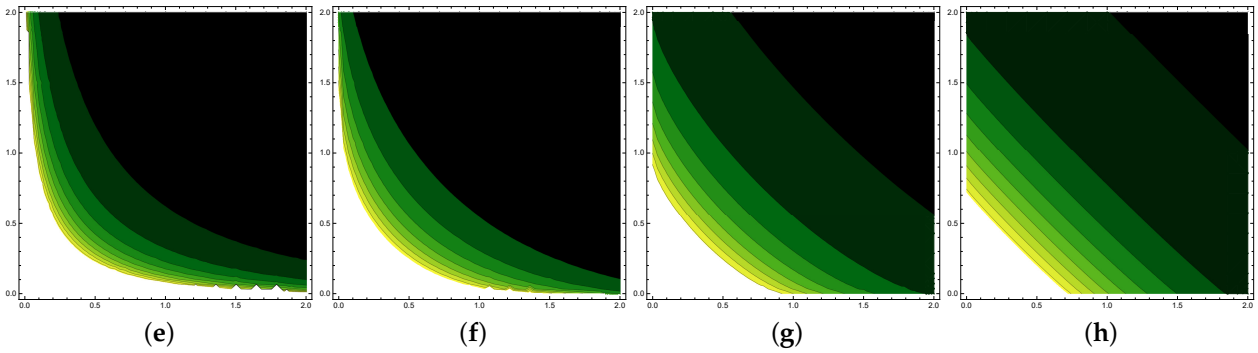

Figure 2. 3D and 2D-Contour graphs for V_6. (**a**) $\alpha = 0.25$. (**b**) $\alpha = 0.50$. (**c**) $\alpha = 0.75$. (**d**) $\alpha = 0.95$. (**e**) $\alpha = 0.25$. (**f**) $\alpha = 0.50$. (**g**) $\alpha = 0.75$. (**h**) $\alpha = 0.95$.

Figures 3 and 4:

A diagram depicts a physical understanding of V_8 that pertains to the domain of semi-dark solutions. Here is a graphical representation of the assessment using the parameters, $b_0 = 0.10714$, $b_1 = -0.03174$, $\mu = \sigma = 1, \nu = -0.0025$, $\beta = 0.035$, $\rho = e$, $m_1 = 1, m_2 = 3$, $m_3 = 2$ with in the interval $(0, 2)$.

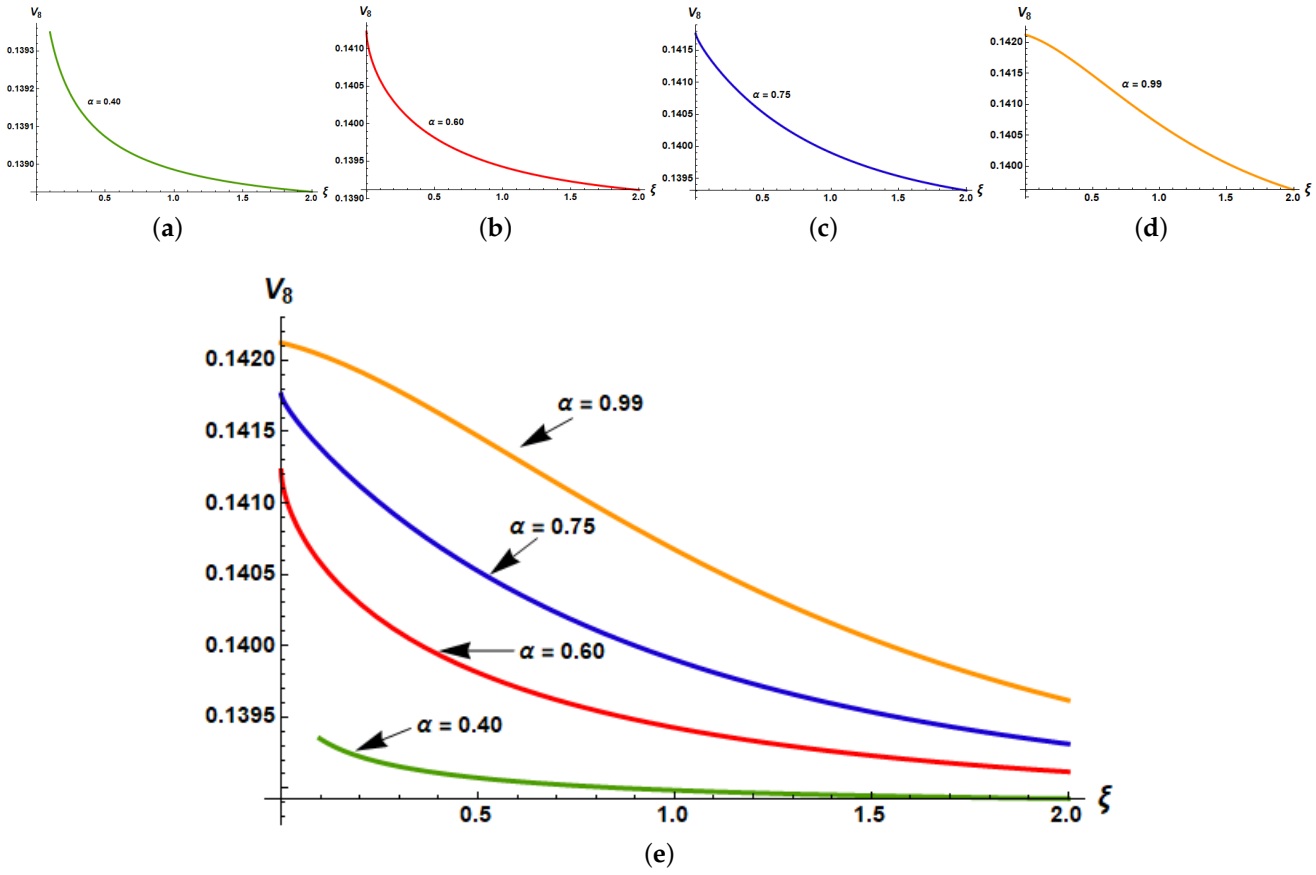

Figure 3. 2D-Graphical representation for V_8. (**a**) $\alpha = 0.40$. (**b**) $\alpha = 0.60$. (**c**) $\alpha = 0.75$. (**d**) $\alpha = 0.99$. (**e**) Combine effect for different fractional values of α.

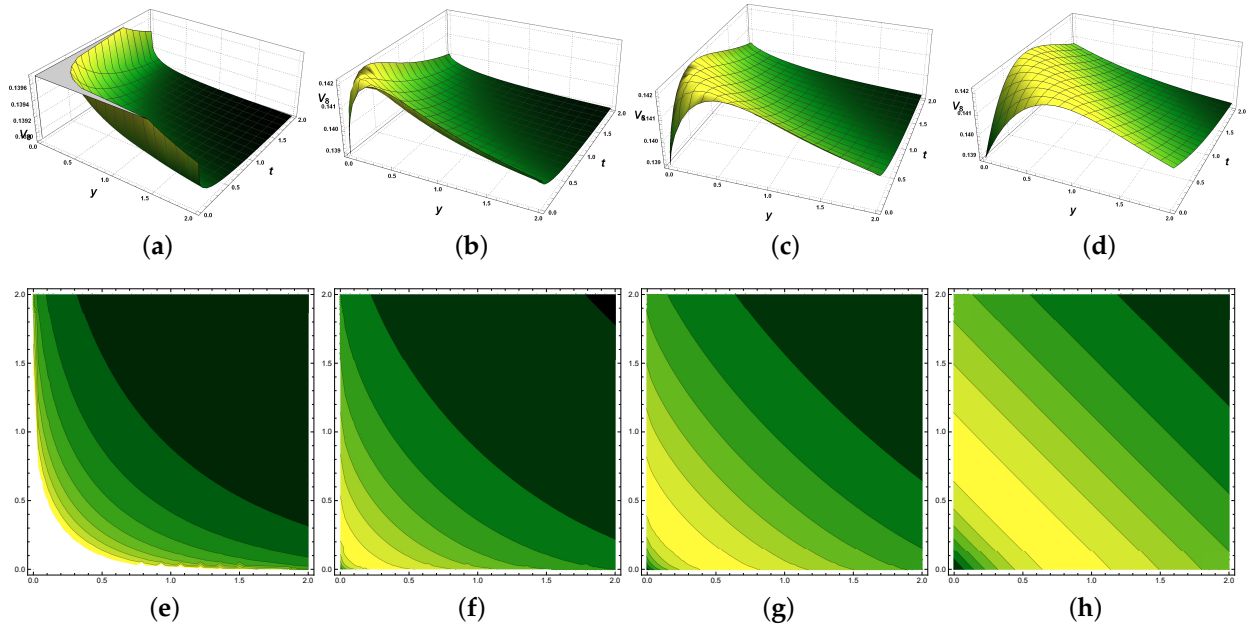

Figure 4. 3D and 2D-Contour graphs for V_8. (**a**) $\alpha = 0.40$. (**b**) $\alpha = 0.60$. (**c**) $\alpha = 0.75$. (**d**) $\alpha = 0.99$. (**e**) $\alpha = 0.40$. (**f**) $\alpha = 0.60$. (**g**) $\alpha = 0.75$. (**h**) $\alpha = 0.99$.

Figures 5 and 6:

This graphic juxtaposes a structural observation of V_{11}. Here is a graphical representation of the inspection using the parameters, $b_0 = 0$, $b_1 = 0.71428$, $\mu = \sigma = 1$, $\nu = -0.0025$, $\beta = 0.035$, $\rho = e$, $m_1 = 1$, $m_2 = 3$, $m_3 = 2$ with in the interval $(0, 2)$.

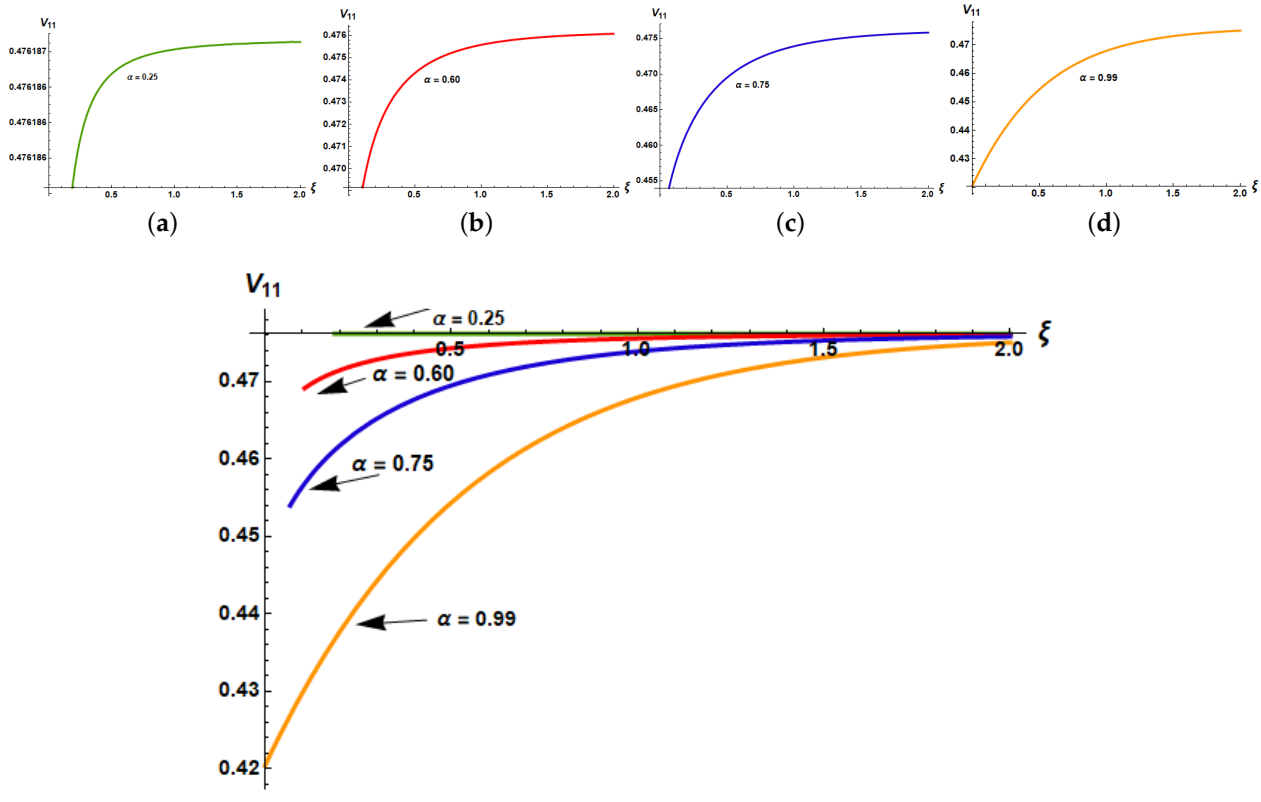

Figure 5. 2D-Graphical representation for V_{11}. (**a**) $\alpha = 0.25$. (**b**) $\alpha = 0.60$. (**c**) $\alpha = 0.75$. (**d**) $\alpha = 0.99$. (**e**) Combine effect for different fractional values of α.

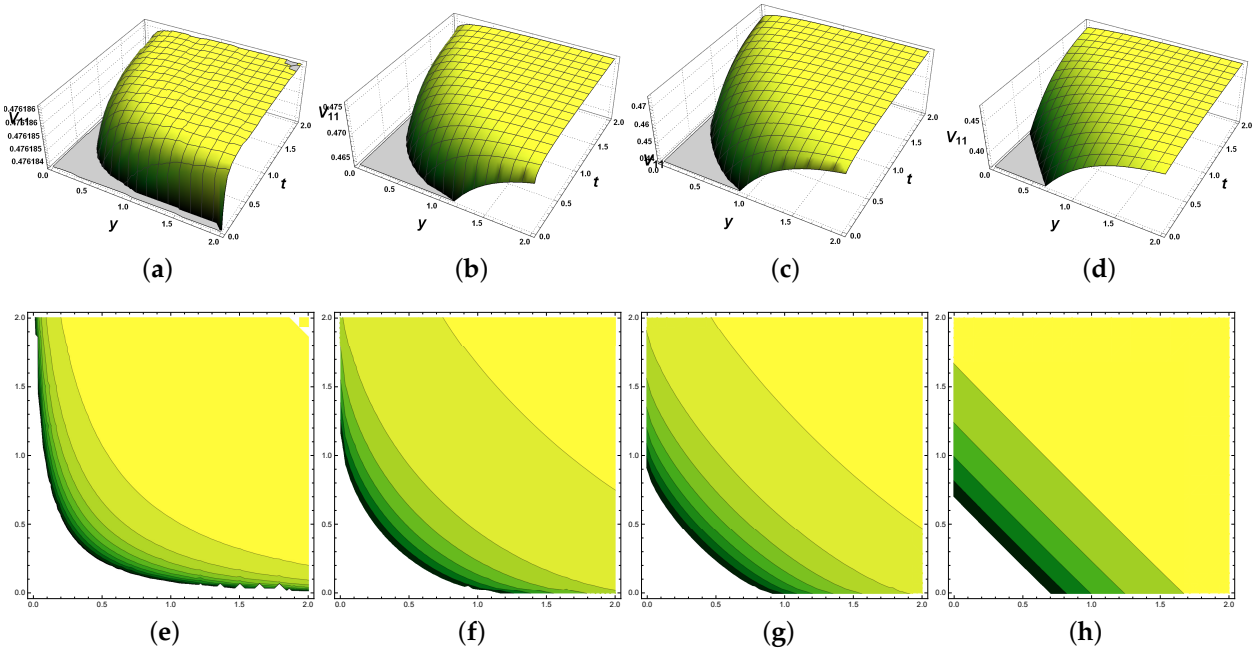

Figure 6. 3D and 2D-Contour graphs for V_{11}. (**a**) $\alpha = 0.25$. (**b**) $\alpha = 0.60$. (**c**) $\alpha = 0.75$. (**d**) $\alpha = 0.99$. (**e**) $\alpha = 0.25$. (**f**) $\alpha = 0.60$. (**g**) $\alpha = 0.75$. (**h**) $\alpha = 0.99$.

Figures 7 and 8:

The graphic juxtaposes a structural observation of V_{13}. Here is a graphical representation of the inspection using the parameters, $\rho = e$, $b_0 = 0, b_1 = 12, \mu = \sigma = 1, \nu = -0.015$, $\beta = -0.0025$, $m_1 = 0$, $m_2 = p = 3$, $m_3 = pq = 9$, $q = p = 3$, $m = n = 1$, with in the interval $(0, 2)$.

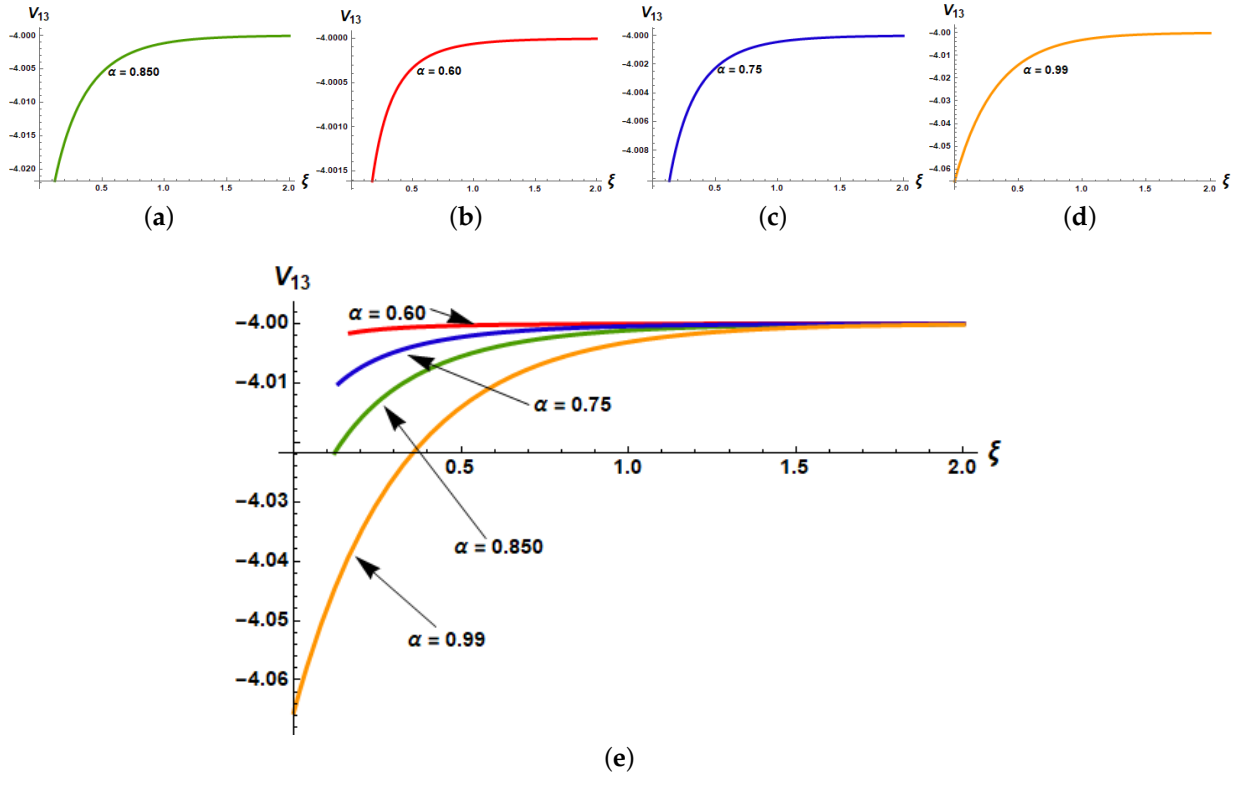

Figure 7. 2D-Graphical representation for V_{13}. (**a**) $\alpha = 0.60$. (**b**) $\alpha = 0.75$. (**c**) $\alpha = 0.85$. (**d**) $\alpha = 0.99$. (**e**) Combine effect for different fractional values of α.

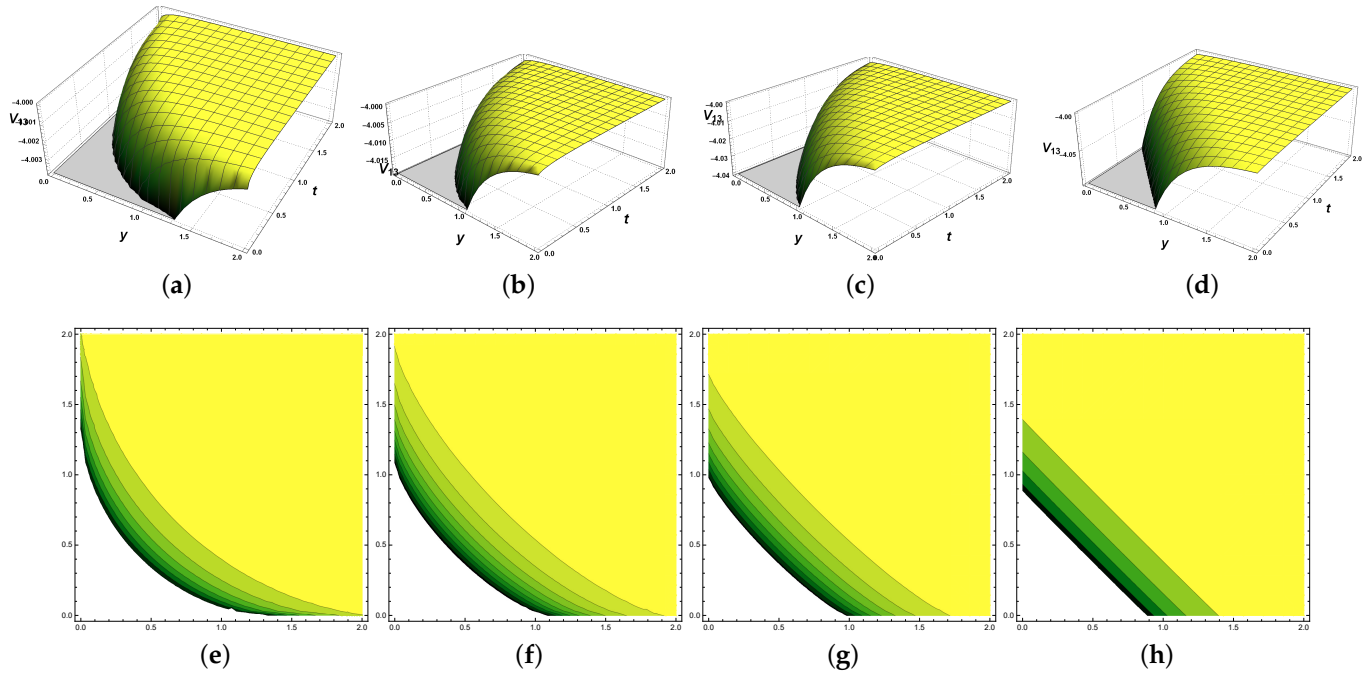

Figure 8. 3Dand 2D-Contour graphs for V_{13}. (**a**) $\alpha = 0.60$. (**b**) $\alpha = 0.75$. (**c**) $\alpha = 0.85$. (**d**) $\alpha = 0.99$. (**e**) $\alpha = 0.60$. (**f**) $\alpha = 0.75$. (**g**) $\alpha = 0.85$. (**h**) $\alpha = 0.99$.

4.1. The Sensitivity Assessment

From Equation (2), we can derive the following system:

$$V'' = \frac{12}{\delta^2\mu^4}(C_0L\sigma^2 - \mu^2)V - \frac{12}{\delta^2\mu^4}C_0L\nu\sigma^2V^2 + \frac{12}{\delta^2\mu^4}C_0L\beta\sigma^2V^3. \tag{8}$$

Equation (8), can be written as:

$$V'' = a_1V + a_2V^2 + a_3V^3, \tag{9}$$

where, $V' = \frac{dV}{d\xi}$, $a_1 = \frac{12}{\delta^2\mu^4}(C_0L\sigma^2 - \mu^2)$, $a_2 = -\frac{12}{\delta^2\mu^4}C_0L\nu\sigma^2$, $a_3 = \frac{12}{\delta^2\mu^4}C_0L\beta\sigma^2$.

Equation (9) may also be expressed by a planer dynamical system using the Galilean transformation, simply:

$$\begin{cases} V' = & w, \\ w' = & a_1V + a_2V^2 + a_3V^3. \end{cases} \tag{10}$$

We shall immediately investigate the sensitive phenomena of the perturbed system shown below. Following that, the schemes Equation (9) is decomposed in the autonomous conservative dynamical system $(ACDS)$, as illustrated below:

$$\begin{cases} V' = & w, \\ w' = & a_1V + a_2V^2 + a_3V^3 + n_0\cos f\xi. \end{cases} \tag{11}$$

In which f appears to be the frequency and n_0 is the strength of the perturbed component [36]. The superficial periodic force can be seen in the system (11); however, not within the system (10). To analyze Equation (2)'s sensitive performance in the emergence of a perturbation component including the parameters a_1, a_2, and a_3. We would investigate how whether the frequency term impacts the model under discussion across the current part of the study. To do so, we shall determine the physical properties of the examined model and explain the impact of the perturbation's force and frequency.

As a result, we wish to investigate the sensitivity of such a solution to the perturbed dynamical structural scheme (11) by applying six unique initial conditions in the component (see Table (1)):

Table 1. Sensitive behaviour of the perturbed system (11).

Figure 9	Red Doted Curve	Solid Blue Line
(a)	(0.00, 0.00)	(0.10, 0.10)
(b)	(0.10, 0.10)	(0.25, 0.25)
(c)	(0.15, 0.15)	(0.20, 0.20)
(d)	(0.35, 0.35)	(0.50, 0.50)
(e)	(0.75, 0.75)	(0.90, 0.90)
(f)	(0.875, 0.875)	(1.30, 1.30)
(g)	(1.00, 1.00)	(1.70, 1.70)

Though the remaining parameters would be the same for every component in Figure 9a–g. The parametric constraints are as follows:

$\rho = e$, $a_1 = 0.1050844884$, $a_2 = 0.0003940668314$, $a_3 = 0.005516935639$, $m_1 = 1$, $m_2 = 3$, $m_3 = 2$, $\beta = -0.035$, $\nu = -0.0025$, $\delta = 15.1125$, $C_0 = 3$, $L = 1$, $f = 4.2$, $n_0 = 0.92$, and $\mu = \sigma = 1$.

The sensitivity test is a procedure for determining how sensitive our system is. The system will have poor sensitivity if it suffers a little change as a result of tiny changes in the starting circumstances. However, if the system is significantly altered as a result of a little change in the original conditions, the system will be extremely vulnerable. The graphs below demonstrate how the amplitude pattern of the waves changes, suggesting that these curves do not overlap, indicating that the system is sensitive in that area.

The Figure 9a plot shows the sensitivity illustrating the dynamical system (11) assuming the similar parameters as stated earlier for the initial constraints as (V, w) = (0, 0) in the red dotted curve and (V, w) = (0.10, 0.10) throughout the solid blue line. The system has very low sensitivity from the beginning (i.e., from 0 to 40) and the system has high sensitivity till the end (i.e., from 40 to 100). Figure 9b shows the sensitivity assuming similar parameters for the initial constraints as (V, w) = (0.10, 0.10) in the red dotted curve and (V, w) = (0.25, 0.25) throughout the solid blue line. The system has very low sensitivity from the beginning (i.e., from 0 to 20) and the system has high sensitivity till the end (i.e., from 20 to 100). Figure 9c shows the sensitivity for the initial constraints (V, w) = (0.15, 0.15) in the red dotted curve and (V, w) = (0.20, 0.20) throughout the solid blue line. The system has very low sensitivity from the beginning (i.e., from 0 to 20) and the system has high sensitivity till the end (i.e., from 20 to 100). For Figure 9d, the initial constraints are as (V, w) = (0.35, 0.35) in the red dotted curve and (V, w) = (0.50, 0.50) throughout the solid blue line. The system has very low sensitivity from the beginning (i.e., from 0 to 50) and the system has high sensitivity till the end (i.e., from 50 to 100). In Figure 9e, (V, w) = (0.75, 0.75) appears as the red dotted curve and (V, w) = (0.90, 0.90) is the solid blue line. The system has very low sensitivity from the beginning (i.e., from 0 to 30) and the system has high sensitivity till the end (i.e., from 30 to 100). Figure 9f shows the sensitivity for the stated initial constraints as (V, w) = (0.875, 0.875) in the red dotted curve and (V, w) = (1.30, 1.30) throughout the solid blue line. The system has very low sensitivity from the beginning (i.e., from 0 to 10) and the system has high sensitivity till the end (i.e., from 10 to 100). The sensitivity for Figure 9g regarding the stated initial constraints as (V, w) = (1.00, 1.00) in the red dotted curve and (V, w) = (1.70, 1.70) throughout the solid blue line. The system has very high sensitivity from the beginning (i.e., from 0 to 70) and the system has low sensitivity till the end (i.e., from 70 to 100).

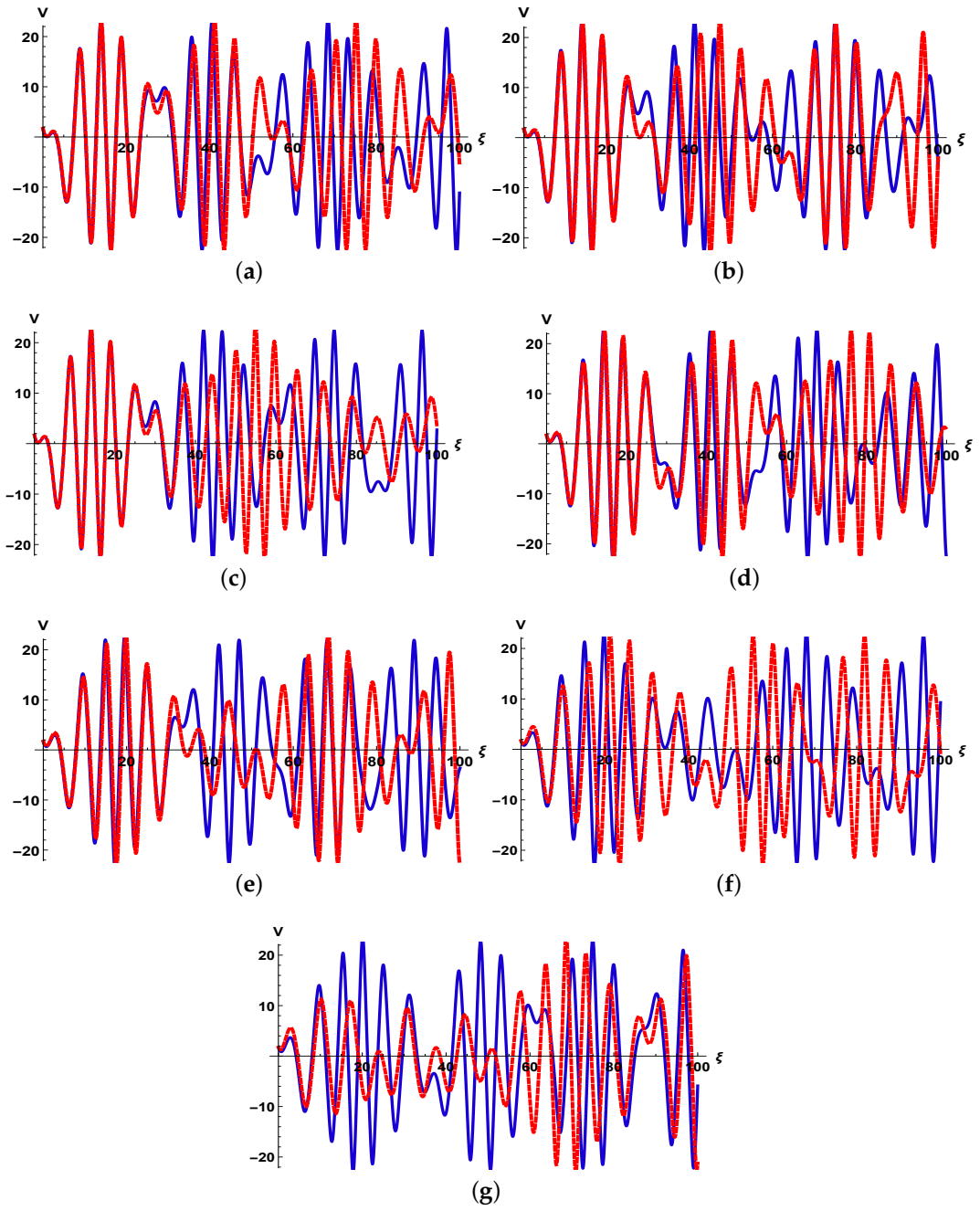

Figure 9. A FO-LPET line model being used to test sensitivity. (**a**) sensitivity illustrating the dynamical system (11) having the same values as stated earlier for the initial constraints as $(V, w) = (0, 0)$ in the red dotted curve and $(V, w) = (0.10, 0.10)$ for the solid blue line. (**b**) sensitivity with initial constraints for red dotted curve and solid blue line with $(V, w) = (0.10, 0.10)$, $(V, w) = (0.25, 0.25)$ respectively. (**c**) $(V, w) = (0.15, 0.15)$ in the red dotted curve and $(V, w) = (0.20, 0.20)$ throughout the solid blue line. (**d**) $(V, w) = (0.35, 0.35)$ in the red dotted curve and (V, w) = (0.50, 0.50). (**e**) (V, w) = (0.75, 0.75) appears as the red dotted curve and $(V, w) = (0.90, 0.90)$ is the solid blue line. (**f**) $(V, w) = (0.875, 0.875)$ in the red dotted curve and (V, w) = (1.30, 1.30). (**g**) $(V, w) = (1.00, 1.00)$ in the red dotted curve and (V, w) = (1.70, 1.70) throughout the solid blue line.

4.2. Quasiperiodic Behaviors

In this subsection, we will look at the quasiperiodic and chaotic dynamics of the perturbed system (11). The superficial periodic force is represented by the system (11), here f is the frequency, and n_0 is the intensity of the perturbed component. It was carried out

to examine the periodic and chaotic behavior of the model in the context of an uncertain perturbation factor. We will look at how the frequency term impacts the model we are looking at in this paper. To do so, we will define the physical properties of the model under investigation and examine the impact of the perturbation's force and frequency.

Figures 10–13 depict a three-dimensional phase picture, Poincar'e section, and time-series graph with different values of f, i.e., the frequency and n_0 is the strength of the perturbed component as already mentioned in the caption of each figure. The perturbed dynamical framework (11) exhibits periodic behavior. While there is a precise arrangement accessible in the Poincar'e section, all of these periodic waves may be observed in the time-series graph, which supports the periodic behavior at such parameter values.

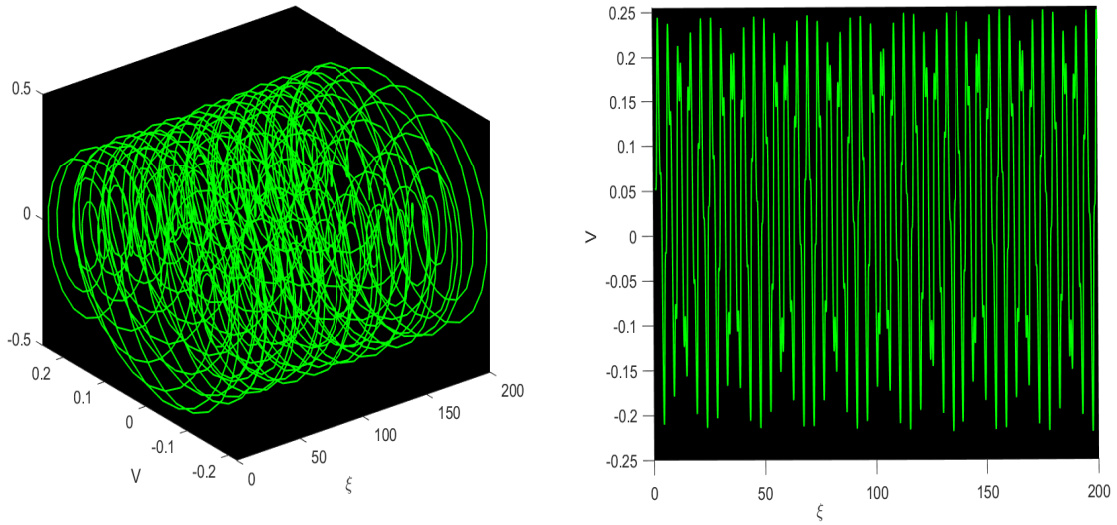

(**a**) (**b**)

Figure 10. Phase-portrait with perturbation term having $a_1 = -2$, $a_2 = 3$, $a_3 = 5$, $n_0 = 0.91$, $f = 4.2$, $\mu = \sigma = 1$, $C_0 = 3$, $L = 1$, $\delta = 12$, $\nu = -1$, $\beta = \frac{5}{3}$ for the dynamical system. (**a**) Phase-portrait with perturbation. (**b**) Poincar'e section.

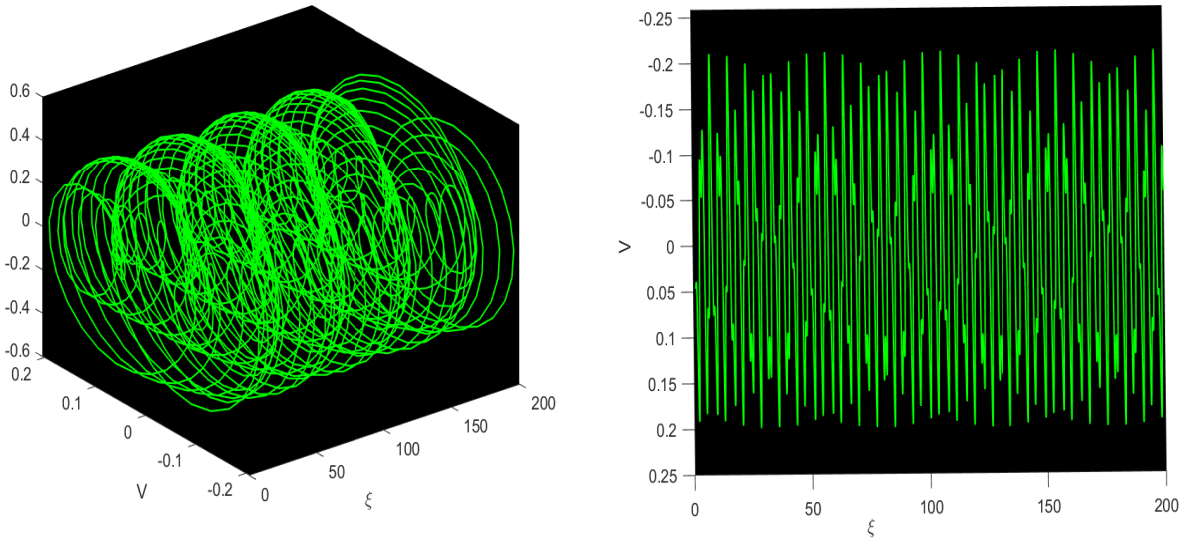

(**a**) (**b**)

Figure 11. Phase-portrait with perturbation term having $a_1 = -3$, $a_2 = 4$, $a_3 = 6$, $n_0 = 0.92$, $f = 4.1$ for the dynamical system. (**a**) Phase-portrait with perturbation. (**b**) Poincar'e section.

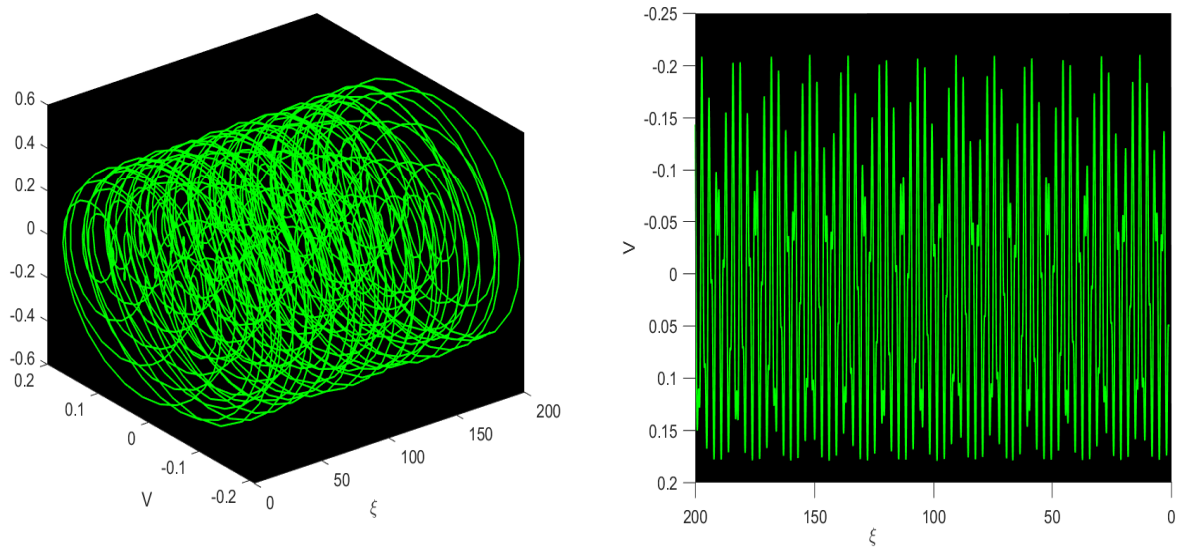

(**a**) (**b**)

Figure 12. Phase-portrait with perturbation term having $a_1 = -4$, $a_2 = 5$, $a_3 = 7$, $n_0 = 0.93$, $f = 4.3$ for the dynamical system. (**a**) Phase-portrait with perturbation. (**b**) Poincar'e section.

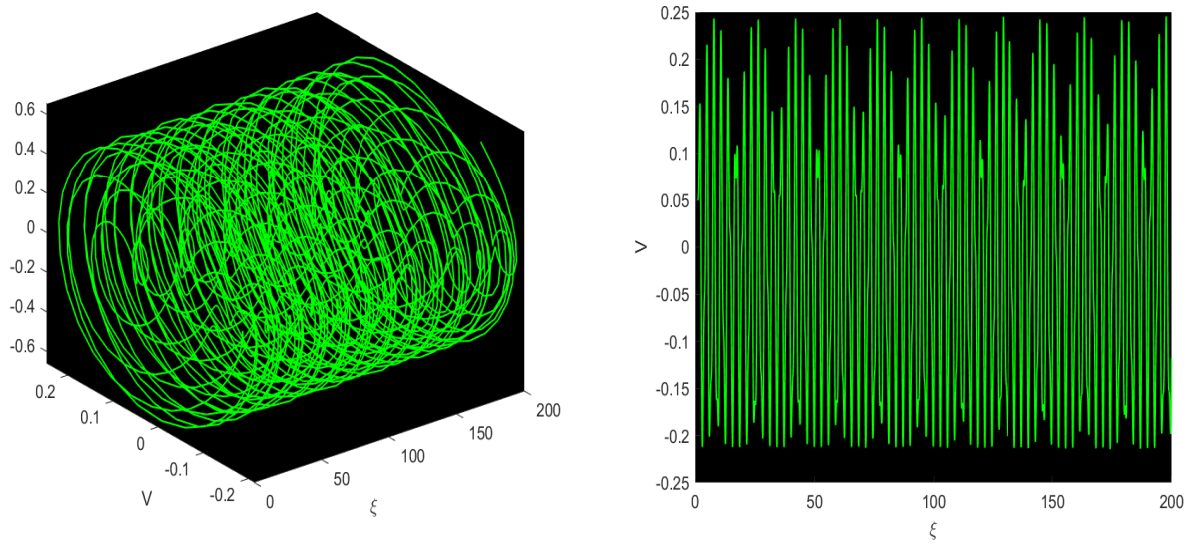

(**a**) (**b**)

Figure 13. Phase-portrait with perturbation term having $a_1 = -4$, $a_2 = -5$, $a_3 = -7$, $n_0 = 0.94$, $f = 4.4$ for the dynamical system. (**a**) Phase-portrait with perturbation. (**b**) Poincar'e section.

5. Discussions and Results Analysis

In [37], the $(\frac{G'}{G^2})$ -expansion approach is used to obtain soliton solutions to the FO differential equation regulating wave propagation in low-pass electrical transmission lines. Because the extended direct algebraic method is more versatile than the $(\frac{G'}{G^2})$ -expansion approach. The extended direct algebraic method provides us with a variety of solitary wave solutions. In this work, a variety of mathematical models were employed and transformed into the same type of ODE, yet resulted in diverse solutions after transformation. We receive the same mathematical functions since the process is similar, but we find distinct visualizations because of distinct parameter's selection.

We offer graphical representations of several sample solutions in this part to explain their physical significance. For gaining new analytical solutions to nonlinear differential equations, the extended direct algebraic approach is very competent and feasible, determining the exact solution in a well-understood manner. It is easier and faster when employing a computation system and is an effective method to tackle the various aspects of analytical solitary solutions. The approach is used to find dark soliton solutions (hyperbolic tangent is arising), semi-dark soliton solutions (both hyperbolic tangent and hyperbolic secant is arising), dark-singular solutions (hyperbolic tangent and hyperbolic cotangent), Type 1 and 2 singular solutions (hyperbolic cotangent and hyperbolic cosecant), Type 2 singular solutions (hyperbolic cotangent), as well as additional LPET line equation solutions. It is pertinent to assert here, based on the conclusions addressed, that now the approach used can effectively address the problem of concern to us through the use of the pragmatic computational program Maple, which might quickly handle the complicated and time-consuming mathematical computations and substantially cut computing time. The graphical results of the aforementioned solutions are shown in Figures 1–8. In exchange for free components of the examined standard model provided Equation (1), the effects of fractionality are discussed in the following subsections via some of the obtained solutions.

The Influence of Fractionality:

The consequences of fractionality are examined using several approaches of the FO-LPET line equation, which are depicted in Figures 1–8 for clarity. The images (Figures 1 and 2) show that when the fractionality increases, the profile takes on the entire form of the dark pattern soliton. In Figures 3 and 4, when the fractionality increases, the shape accomplishes the semi-bright feature soliton's appearance. Furthermore, in Figures 5 and 6, it is apparent that when the fractionality increases, the amplitudes of the wave solutions drop, as seen by their trajectories. The graphs in Figures 7 and 8 indicate that when fractionality rises, the amplitudes of the wave solution grow as well.

The Influence of unrestricted parameters:

The impacts of the model equation's unrestricted parameters via solution V_8, which is a semi-dark solution, can be seen in Figures 14 and 15. To obtain the figures, several variations of the unrestricted components are used.

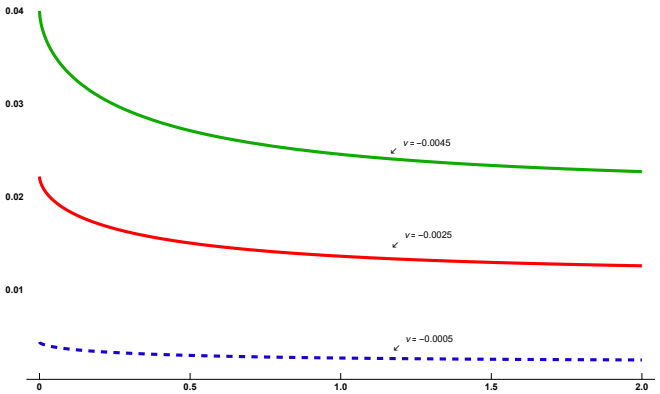

Figure 14. Combine influence for different values of free parameter ν.

Considering such statistics, it is clear from Figure 13 that the levels of intensity of the semi-bright wave profiles drop as ν, where $\nu < 0$ increases.

Since these facts are taken into account, it is evident from Figure 14 that the levels of intensity of the semi-bright wave description grow as β, where $\beta > 0$ declines. Based on the preceding explanation, this is fair to deduce that the negative and positive amount of the model's non-linearity elements, i.e., ν and β can have an impact on raising and reducing the wave profile intensity.

In the "the sensitivity assessment" part, we can observe the sensitivity appraisal for Equation (1) of the perturbed dynamical structural network (11) by adopting seven unique beginning conditions in Figure 9a–g. A sensitivity evaluation is a test that assesses the

level of sensitivity in our network. The network will have low sensitivity if it suffers a little modification as a consequence of minor changes in the starting circumstances. The system, on the other hand, will be extremely sensitive if it endures a considerable modification as a consequence of minor changes in the original circumstances. These people will surely make a significant contribution to this virtue. Soliton offers a wide variety of applications in science and engineering.

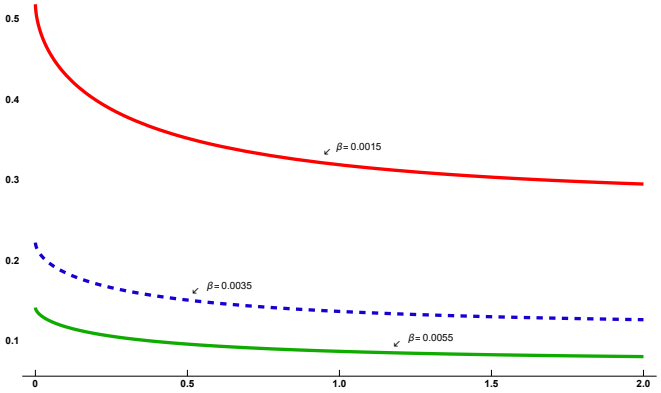

Figure 15. Combine influence for different values of free parameter β.

The superficial periodic force is represented by the system (11), where f is the frequency, and n_0 is the intensity of the perturbed component. The perturbed dynamical structure (11) is thought to exhibit quasiperiodic-chaotic behavior in Figures 10–13. The points on the Poincar'e section are dispersed, yet they have a different profile for such values, indicating that there is a quasi-periodic structure for that specific parameter values.

6. Comparative Analysis via Different FDs

Because of the different descriptions of FDs (conformable derivative (CD), modified Riemann-Liouville (mRL), beta derivation (BD), etc.), fractional form solutions offer unique graphical observations and applications when the fractional value of these FDs is taken into account. It is exceedingly challenging for scientists to determine which of the FDs is the most accurate and reliable. In this part, meanwhile, a comparison of the outcomes found during this research with many others derived by the use of the mRL and BD is provided. Teodoro et al. and [5,38] conducted a thorough examination of the descriptions and characteristics of mRL and BD and a comparative study of the optical solitons of the FO complex GL equation with conformable, M-truncated, and beta derivatives. It should be noted that the transformations take place here, $v(x,t) = V(\xi)$, $\xi = \mu\frac{x^{\alpha}}{\Gamma(1+\alpha)} + \sigma\frac{t^{\alpha}}{\Gamma(1+\alpha)}$, for mRL derivation, and $v(x,t) = V(\xi)$, $\xi = \frac{\mu}{\alpha}\left(x + \frac{1}{\Gamma(\alpha)}\right)^{\alpha} + \frac{\sigma}{\alpha}\left(t + \frac{1}{\Gamma(\alpha)}\right)^{\alpha}$, for the BD are utilised for Equation (1) and after integrating the resultant equation two times and reducing the integrating constants to zero, the ODE described by Equation (2) is derived. Two wave solutions are provided in each case to compare the performance of the findings produced in this analysis with those achieved using the mRL derivative and BD. The solutions Equations V_6, V_8, and V_{13} produced with the sense of the CD are created with the concept of the mRL derivative and BD, respectively, and thus are stated as follows:

We provide the findings by the corresponding FD in Figures 16–18 to compare the accuracy and reliability of our generated solutions via the CD with those acquired by the mRL derivative and BD. The trend of all of the solution profiles for the stated derivatives can be seen in all these figures above, but the solutions produced in this investigation can be determined to be in good correlation with those derivatives. As a result, it is possible to verify that the solutions obtained with the CD are in between both of the derivatives, i.e., the mRL derivative and BD.

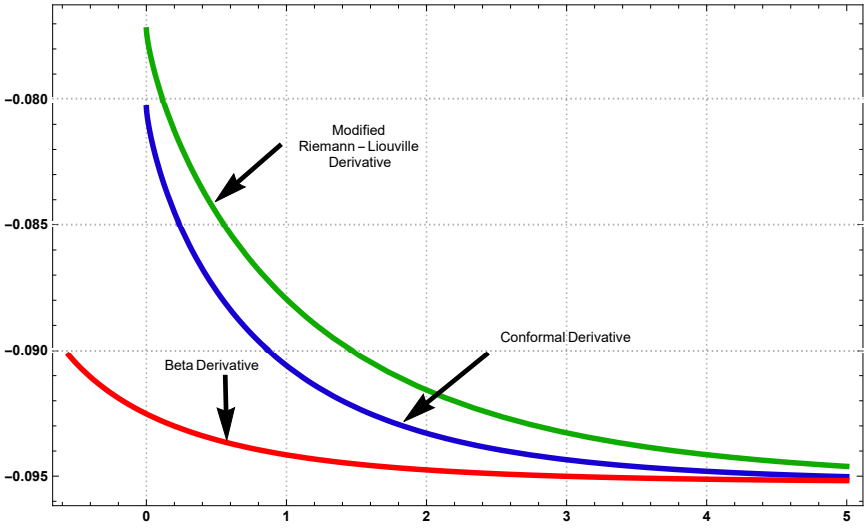

Figure 16. Comparative investigation of the dark soliton solution (V_6) via the mRL derivative, CD and BD's for the fix value of FO $\alpha = 0.75$ defined by these FDs.

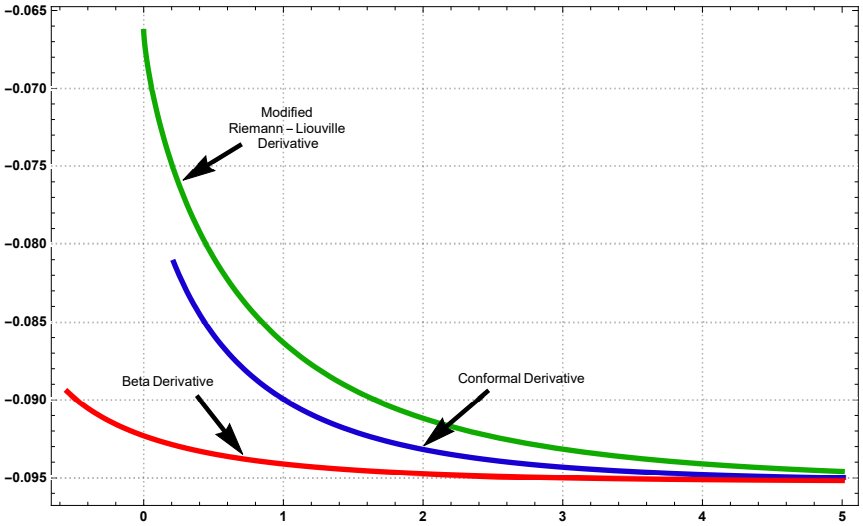

Figure 17. Comparative investigation of the semi-dark soliton solution (V_8) via the mRL derivative, CD and BD's for the fix value of FO $\alpha = 0.75$ defined by these FDs.

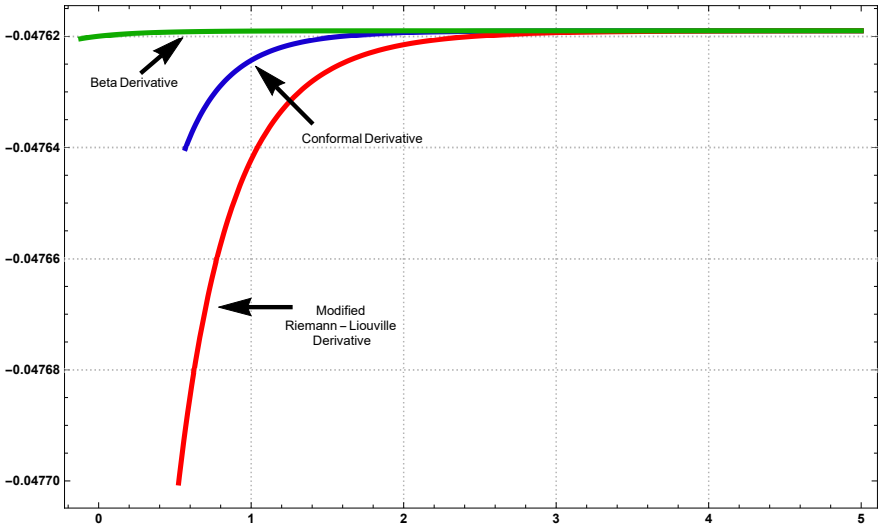

Figure 18. Comparative investigation of the soliton solution (V_{13}) via the mRL derivative, CD and BD's for the fix value of FO $\alpha = 0.75$ defined by these FDs.

There exist a comparable number of articles in the literature with particularly good results. Here, we write a short comparison with this article [39]. Here in this paper, the results were obtained by factorization and written in terms of the Weierstrass function. For particular values of the involved parameters, few results are shown in terms of the hyperbolic and trigonometric functions. On the other hand, we have more general results in the form of hyperbolic, trigonometric, exponential, and rational. Moreover, we obtain the bright, dark, periodic, singular, and other soliton solutions to this nonlinear model.

7. Conclusions

We have retrieved the trigonometric, mixed hyperbolic, and rational soliton structure to the NLEEs characterizing wave motion in nonlinear LPET lines using the extended direct algebraic method with fractional transformation. We have displayed some obtained ideal solutions in 2D, and 3D layouts, including dark soliton solutions, the representatives of the semi-bright soliton solutions, dark singular, singular solitons of *Type* 1, and soliton outcomes by picking appropriate values for the free parameters, and examined the repercussions of fractionality as well as the unrestricted factors of the model equation. The effects of fractionality have been investigated utilizing graphical representations of different solutions to the FO-LPET line problem. When the fractionality $(0 < \alpha < 1)$ rises, the amplitude either increases or drops. Relying on the explanation mentioned earlier, It makes sense to assume that negative and positive values of the model's nonlinearity elements, ν along with β, can influence the intensity of the wave characteristics. Moreover, a comparison was performed between the findings obtained in this research and those obtained using the same approach while considering the FDs in terms of the modified Riemann-Liouville and beta derivation. We discussed sensitivity assessment. A sensitivity evaluation is a test that assesses the sensitivity of our system. If the system suffers a minor change due to minor modifications in the starting conditions, the system will have low sensitivity. We, however, still examined how our model's perturbed dynamical framework exhibits quasiperiodic-chaotic characteristics. The validity of the resultant outcomes was tested by re-entering the obtained solutions into the equation of our choice using computer software. As a result, the entire study shows that such implemented approach is an effective productivity tool for achieving a diverse variety of traveling wave solutions to NLEEs in science, engineering, and mathematical physics. Because solitons may be used in telecommunication systems to communicate information and increase information data rates, the findings of such a study may be valuable in studying the soliton solutions of LPET lines. Solitons' capacity to travel with low dispersion can be utilized to send data modulated as brief pulses over vast ranges. One of the productive frameworks for discussing the many kinds of exact optical solitary solutions is the extended direct algebraic method. the sufficient conditions for the stability of the results, which refers to the situation where a minor disruption inside a system does not have a significant impact on the system, is also discussed. A quick and straightforward assessment reveals that the offered solutions are unique and special. The study's findings presented in this paper are novel and have never been published before.

Author Contributions: The authors have contributed equally to this work. All authors have read and agreed to the published version of the manuscript.

Funding: This research receives no external funding.

Conflicts of Interest: The authors declare no conflicts of interest.

References

1. Atangana, A.; Secer, A. A note on fractional order derivatives and table of fractional derivatives of some special functions. *Abstr. Appl. Anal.* **2013**, *2013*, 279681. [CrossRef]
2. Yang, X.J.; Machado, J.T.; Hristov, J. Nonlinear dynamics for local fractional Burgers' equation arising in fractal flow. *Nonlinear Dyn.* **2016**, *84*, 3–7. [CrossRef]

3. Park, C.; Khater, M.M.; Attia, R.A.; Alharbi, W.; Alodhaibi, S.S. An explicit plethora of solution for the fractional nonlinear model of the low–pass electrical transmission lines via Atangana–Baleanu derivative operator. *Alex. Eng. J.* **2020**, *59*, 1205–1214. [CrossRef]
4. El-Wakil, S.A.; Abulwafa, E.M. Formulation and solution of space–time fractional Boussinesq equation. *Nonlinear Dyn.* **2015**, *80*, 167–175. [CrossRef]
5. Teodoro, G.S.; Machado, J.T.; De Oliveira, E.C. A review of definitions of fractional derivatives and other operators. *J. Comput. Phys.* **2019**, *388*, 195–208. [CrossRef]
6. Yepez-Martinez, H.; Gómez-Aguilar, J.F. Optical solitons solution of resonance nonlinear Schrödinger type equation with Atangana's-conformable derivative using sub-equation method. *Waves Random Complex Media* **2021**, *31*, 573–596. [CrossRef]
7. Uchaikin, V.V. *Fractional Derivatives for Physicists and Engineers*; Springer: Berlin, Germany, 2013; Volume 2.
8. Zhao, D.; Luo, M. General conformable fractional derivative and its physical interpretation. *Calcolo* **2017**, *54*, 903–917. [CrossRef]
9. Khalil, R.; Al Horani, M.; Yousef, A.; Sababheh, M. A new definition of fractional derivative. *J. Comput. Appl. Math.* **2014**, *264*, 65–70. [CrossRef]
10. Osman, M.S.; Rezazadeh, H.; Eslami, M. Traveling wave solutions for (3 + 1) dimensional conformable fractional Zakharov-Kuznetsov equation with power law nonlinearity. *Nonlinear Eng.* **2019**, *8*, 559–567. [CrossRef]
11. Kumar, D.; Paul, G.C.; Mondal, J.; Islam, A.S. On the propagation of alphabetic-shaped solitons to the (2 + 1)-dimensional fractional electrical transmission line model with wave obliqueness. *Results Phys.* **2020**, *19*, 103641. [CrossRef]
12. Qu, H.; She, Z.; Liu, X. Homotopy analysis method for three types of fractional partial differential equations. *Complexity* **2020**, *2020*, 7232907. [CrossRef]
13. Liu, J.G.; Yang, X.J.; Feng, Y.Y.; Cui, P. On the (N + 1)-dimensional local fractional reduced differential transform method and its applications. *Math. Methods Appl. Sci.* **2020**, *43*, 8856–8866. [CrossRef]
14. Javeed, S.; Baleanu, D.; Waheed, A.; Shaukat Khan, M.; Affan, H. Analysis of homotopy perturbation method for solving fractional order differential equations. *Mathematics* **2019**, *7*, 40. [CrossRef]
15. Prakash, A.; Goyal, M.; Gupta, S. Fractional variational iteration method for solving time-fractional Newell-Whitehead-Segel equation. *Nonlinear Eng.* **2019**, *8*, 164–171. [CrossRef]
16. Li, W.; Pang, Y. Application of Adomian decomposition method to nonlinear systems. *Adv. Differ. Equ.* **2020**, *2020*, 67. [CrossRef]
17. Mirzazadeh, M.; Eslami, M.; Biswas, A. Soliton solutions of the generalized Klein–Gordon equation by using $\left(\frac{G'}{G}\right)$-expansion method. *Comput. Appl. Math.* **2014**, *33*, 831–839. [CrossRef]
18. Ayub, K.; Khan, M.Y.; Hassan, Q.M.U.; Yasmeen, F.; Saleem, M.; Mansoor, M. On an efficient technique to solve nonlinear fractional order partial differential equations. *J. Sci. Arts* **2018**, *18*, 565–572.
19. Kaplan, M.; Akbulut, A.; Bekir, A. Solving space-time fractional differential equations by using modified simple equation method. *Commun. Theor. Phys.* **2016**, *65*, 563. [CrossRef]
20. Savaissou, N.; Gambo, B.; Rezazadeh, H.; Bekir, A.; Doka, S.Y. Exact optical solitons to the perturbed nonlinear Schrödinger equation with dual-power law of non-linearity. *Opt. Quantum Electron.* **2020**, *52*, 318. [CrossRef]
21. Kumar, D.; Seadawy, A.R.; Haque, M.R. Multiple soliton solutions of the nonlinear partial differential equations describing the wave propagation in nonlinear low–pass electrical transmission lines. *Chaos Solitons Fractals* **2018**, *115*, 62–76. [CrossRef]
22. Kumar, D.; Seadawy, A.R.; Chowdhury, R. On new complex soliton structures of the nonlinear partial differential equation describing the pulse narrowing nonlinear transmission lines. *Opt. Quantum Electron.* **2018**, *50*, 108. [CrossRef]
23. Akbulut, A.; Kaplan, M. Auxiliary equation method for time-fractional differential equations with conformable derivative. *Comput. Math. Appl.* **2018**, *75*, 876–882. [CrossRef]
24. Kumar, D.; Paul, G.C.; Biswas, T.; Seadawy, A.R.; Baowali, R.; Kamal, M.; Rezazadeh, H. Optical solutions to the Kundu-Mukherjee-Naskar equation: Mathematical and graphical analysis with oblique wave propagation. *Phys. Scr.* **2020**, *96*, 025218. [CrossRef]
25. Mohyud-Din, S.T.; Bibi, S. Exact solutions for nonlinear fractional differential equations using $\left(\frac{G'}{G^2}\right)$-expansion method. *Alex. Eng. J.* **2018**, *57*, 1003–1008. [CrossRef]
26. Arqub, O.A.; Al-Smadi, M.; Almusawa, H.; Baleanu, D.; Hayat, T.; Alhodaly, M.; Osman, M.S. A novel analytical algorithm for generalized fifth-order time-fractional nonlinear evolution equations with conformable time derivative arising in shallow water waves. *Alex. Eng. J.* **2022**, *61*, 5753–5769. [CrossRef]
27. Ali, F.; Jhangeer, A.; Muddassar, M.; Almusawa, H. Solitonic, quasi-periodic, super nonlinear and chaotic behaviors of a dispersive extended nonlinear Schrödinger equation in an optical fiber. *Results Phys.* **2021**, *31*, 104921. [CrossRef]
28. Sabir, Z.; Munawar, M.; Abdelkawy, M.A.; Raja, M.A.Z.; Ünlü, C; Jeelani, M.B.; Alnahdi, A.S. Numerical Investigations of the Fractional-Order Mathematical Model Underlying Immune-Chemotherapeutic Treatment for Breast Cancer Using the Neural Networks. *Fractal Fract.* **2022**, *6*, 184. [CrossRef]
29. Almusawa, H.; Nur Alam, M.; Fayz-Al-Asad, M.; Osman, M.S. New soliton configurations for two different models related to the nonlinear Schrödinger equation through a graded-index waveguide. *AIP Adv.* **2021**, *11*, 065320. [CrossRef]
30. Malik, S.; Almusawa, H.; Kumar, S.; Wazwaz, A.M.; Osman, M.S. A (2 + 1)-dimensional Kadomtsev–Petviashvili equation with competing dispersion effect: Painlevé analysis, dynamical behavior and invariant solutions. *Results Phys.* **2021**, *23*, 104043. [CrossRef]

31. Kundu, P.R.; Almusawa, H.; Fahim, M.R.A.; Islam, M.E.; Akbar, M.A.; Osman, M.S. Linear and nonlinear effects analysis on wave profiles in optics and quantum physics. *Results Phys.* **2021**, *23*, 103995. [CrossRef]
32. Jhangeer, A.; Munawar, M.; Riaz, M.B.; Baleanu, D. Construction of traveling waves patterns of $(1+n)$-dimensional modified Zakharov-Kuznetsov equation in plasma physics. *Results Phys.* **2020**, *19*, 103330. [CrossRef]
33. Munawar, M.; Jhangeer, A.; Pervaiz, A.; Ibraheem, F. New general extended direct algebraic approach for optical solitons of Biswas-Arshed equation through birefringent fibers. *Optik* **2021**, *228*, 165790. [CrossRef]
34. Jhangeer, A.; Munawar, M.; Atangana, A.; Riaz, M.B. Analysis of electron acoustic waves interaction in the presence of homogeneous unmagnetized collision-free plasma. *Phys. Scr.* **2021**, *96*, 075603. [CrossRef]
35. Abdou, M.A.; Soliman, A.A. New exact travelling wave solutions for space-time fractional nonlinear equations describing nonlinear transmission lines. *Results Phys*. **2018**, *9*, 1497–1501. [CrossRef]
36. Jhangeer, A.; Hussain, A.; Tahir, S.; Sharif, S. Solitonic, super nonlinear, periodic, quasiperiodic, chaotic waves and conservation laws of modified Zakharov-Kuznetsov equation in transmission line. Commun. *Nonlinear Sci. Numer. Simul.* **2020**, *86*, 105254. [CrossRef]
37. Nuruzzaman, M.; Kumar, D.; Paul, G.C. Fractional low-pass electrical transmission line model: Dynamic behaviors of exact solutions with the impact of fractionality and free parameters. *Results Phys.* **2021**, *27*, 104457. [CrossRef]
38. Hussain, A.; Jhangeer, A.; Abbas, N.; Khan, I.; Sherif, E.S.M. Optical solitons of fractional complex Ginzburg–Landau equation with conformable, beta, and M-truncated derivatives: A comparative study. *Adv. Differ. Equ.* **2020**, *2020*, 612. [CrossRef]
39. Estévez, P.G.; Kuru, Ş.; Negro, J.; Nieto, L.M. Solutions of a class of Duffing oscillators with variable coefficients. *Int. J. Theor. Phys.* **2011**, *50*, 2046–2056. [CrossRef]